

1 **This manuscript is a preprint** and has been accepted for publication in **Geo-**
2 **physical Research Letters**. The final version of this manuscript is available via the
3 'Peer-reviewed Publication DOI' link on the right-hand side of this webpage. Please feel
4 free to contact any of the authors; we welcome feedback.

5 **Fluid surface coverage showing the controls of rock** 6 **mineralogy on the wetting state**

7 **Gaetano Garfi¹, Cédric M. John¹, Qingyang Lin¹, Steffen Berg^{1,2}, Samuel**
8 **Krevor¹**

9 ¹Imperial College London, Department of Earth Science and Engineering, London, UK

10 ²Shell Global Solutions International B.V., Amsterdam, The Netherlands and Imperial College London,

11 Department of Earth Sciences and Engineering, Department of Chemical Engineering, London, UK

12 **Key Points:**

- 13 • The analysis of fluid surface coverage is proposed as a novel approach to rock wet-
14 tability characterisation
- 15 • A thermodynamically constrained model is derived and tested on a Bentheimer
16 sandstone water-wet X-ray micro-CT dataset
- 17 • In a Berea sandstone, fluid surface coverage shows that rock mineralogy controls
18 system local wettability after exposure to crude oil

Corresponding author: Gaetano Garfi, g.garfi17@imperial.ac.uk

Abstract

The wetting state is an important control on flow in subsurface multi fluid phase systems, e.g., carbon storage and oil production. Advances in X-ray imaging allow us to characterise the wetting state using imagery of fluid arrangement within the pores of rocks. We derived a model from equilibrium thermodynamics relating fluid coverage of rock surfaces to wettability and fluid saturation. The model reproduces the behaviour measured in a water-wet, nearly all-quartz, Bentheimer sandstone imaged during steady-state imbibition. A shift in fluid surface coverage is observed when the rock is altered to a new wetting state with crude oil. In two multi-mineralogical (Berea) samples, one water-wet and the other altered with crude oil, the analysis of fluid surface coverage after imbibition revealed mineral specific wetting preferences only in the altered system. Clays and calcite preferentially alter to an oil-wet state, leading to mixed wettability in the rock.

Plain Language Summary

The movement of multiple fluid phases through the pores of rocks is central to many processes of scientific and societal interest, e.g., CO₂ storage, oil production. When two or more fluids occupies rock pores, the way these fluids move strongly depends on the way the fluids interact with the mineral surfaces constituting rock pore walls. In general, the mineral surfaces prefer to be in contact with one particular fluid. This wetting preference controls the flow of these fluids across large scales in the subsurface.

In this work, we proposed a theoretical and practical approach to characterise this wetting preference. Our approach is based on the analysis of the interfaces shared by rock surfaces with each fluid. The extent of these interfaces depends on rock grains wetting preference. Since this preference can be modified by exposing certain rock samples to crude oil, we prove that the fluid-rock interfaces change accordingly in a rock constituted by a single mineralogy. Finally, we investigate mineral wetting preference, in a rock comprising multiple minerals. When previously exposed to crude oil, these minerals show a different wetting preference. This behaviour is not observed when a sample of the same kind was not exposed to crude oil.

1 Introduction

Wettability is an important control in subsurface fluid flow, where fluids move through pore networks where capillary forces are dominant (Zou et al., 2018; Rücker et al., 2019; Lin, Bijeljic, Berg, et al., 2019). During oil recovery rock wettability exerts a control on the capillary entry pressure during primary drainage or in determining the likelihood of snap-off events of the non-wetting phase during waterflooding (Blunt et al., 2002). As a consequence of pore scale fluid dynamics, the behaviours of continuum scale properties such as relative permeability and capillary pressure are controlled by the wetting state (Anderson, 1987a, 1987b).

Predicting and characterising the wettability of a reservoir is a complex task. Minerals constituting rocks are naturally water-wet in the absence of hydrocarbon deposits. However, many oil reservoirs show relative permeability and capillary pressure functions indicative of intermediate-wet, mixed-wet or oil-wet systems (Donaldson et al., 1969). Indeed, rock surface wetting preference may be altered by the interaction of the solid substrate with surface-active compounds present in the crude oil. If present, these compounds can precipitate or diffuse to the solid surface and be adsorbed modifying the local wetting state (J. S. Buckley & Liu, 1998; J. S. Buckley, 1998). The results of these alteration mechanisms are dependent on the thermodynamic conditions, crude oil composition, brine composition and solid surface chemistry.

66 A number of studies have characterised the wetting behaviour of minerals typically
67 found in the subsurface, i.e., in carbonate and sandstone reservoirs. A summary of the
68 results of a collection of studies can be found in J. S. Buckley (1998). Calcite and clay
69 minerals have been found to be more responsive to wettability alteration by crude oil
70 exposure than quartz (Alipour Tabrizy et al., 2011). However, experiments on chemi-
71 cally homogeneous flat surfaces or powders can only reproduce uniform altered wetta-
72 bility in the system considered. In order to investigate the role of rock textural complex-
73 ity, petrography and mineralogical heterogeneity in determining the *in situ* wetting state,
74 it is necessary to study three-dimensional samples.

75 X-ray micro-CT offers the opportunity to investigate fluid arrangement inside rock
76 pores (Bultreys, Boone, et al., 2016; Bultreys, De Boever, & Cnudde, 2016; Coles et al.,
77 1996). With this newfound capability, thermodynamic theory indicates that it should
78 be possible to observe wetting signals from *in situ* contact angles, interfacial fluid cur-
79 vature and fluid-solid surface coverage (Morrow & Szabo, 1970). *In situ* contact angles
80 have been measured - either manually (Andrew et al., 2014; Singh et al., 2016) or au-
81 tomatically (Klise et al., 2016; Scanziani et al., 2017; AlRatrouf et al., 2017) - in the pore
82 space of various rock samples identifying different wetting states (Rücker et al., 2019;
83 Alhammadi et al., 2017). However, the measurements typically obtained have shown a
84 large variability in space and sensitivity to the processing pipeline chosen (Garfi et al.,
85 2019), making their direct employment difficult. Mean interfacial fluid curvature has suc-
86 cessfully been employed to map capillary pressure in water-wet and intermediate-wet rock
87 samples (Herring et al., 2017; Garing et al., 2017; Lin et al., 2018a; Lin, Bijeljic, Berg,
88 et al., 2019). However, the interpretation of mean interfacial curvature as a signal of wet-
89 ting is not straightforward: when the system is not water-wet, interfaces tend to have
90 null mean curvature, meaning that their curvature has opposite sign along the two prin-
91 cipal radii of curvature (Lin, Bijeljic, Berg, et al., 2019). The fluid-solid surface cover-
92 age is investigated in this study. The measurement of fluid-solid interfacial area bene-
93 fits from a larger signal (more pixels in the imagery) than the contact angle. It also al-
94 lows a more direct interpretation than measurements of both contact angle and fluid-
95 fluid interfacial curvature (Garfi et al., 2019).

96 In this study, we show that the characterisation of fluid coverage of rock mineral
97 surfaces can depict changes in the local wetting state. We develop and validate a model,
98 based in the equilibrium thermodynamics of fluid-solid interfaces of a water-wet system,
99 to demonstrate the applicability of solid surface coverage as a measure of wetting. Fluid-
100 solid interfacial areas are then measured to characterise the wetting state of two rock litholo-
101 gies. We first make use of observations on a mono-mineralogical rock (Bentheimer sand-
102 stone) as a case study to test the approach. We then extend our approach to the min-
103 eralogically heterogeneous Berea sandstone. We investigate mineral specific wettability
104 in two Berea sandstone samples - one in its original state and one exposed to crude oil
105 to alter the natural mineral wetting preference - by performing two drainage-waterflooding
106 cycle experiments and comparing the fluid arrangement observed in the two images ac-
107 quired after waterflooding.

108 2 Materials and Methods

109 2.1 Mono-mineralogical system: Bentheimer sandstone datasets

110 In this work we first make use of two datasets created by Lin et al. (2018a) and Lin,
111 Bijeljic, Berg, et al. (2019) as a case study with a simplified mineralogy. Bentheimer sand-
112 stone is 98 wt% quartz, 1 wt% kaolinite/chlorite and 1 wt% microcline, but for the pur-
113 poses of this work it was assumed to be a homogeneous rock constituted of a single min-
114 eralogy. All the images were segmented into rock, brine and oil phases (Lin et al., 2018a;
115 Lin, Bijeljic, Berg, et al., 2019). In our study the region of interest used in the analy-

116 sis was $900 \times 900 \times 3000$ voxels with $3.58 \mu\text{m}$ voxel side, i.e. the spatial domain anal-
 117 ysed was $3.22 \times 3.22 \times 10.74 \text{mm}^3$.

118 The first dataset - that we call Bentheimer Unaltered - consisted of the X-ray micro-
 119 CT images acquired with two-fluid injection at five fractional flows ($f_w = q_w / (q_w +$
 120 $q_o)$ where q_i are volume flow rates of brine and oil) (S. Buckley & Leverett, 1942) of the
 121 wetting phase, brine phase ($f_w = \{0.15, 0.30, 0.50, 0.85, 1\}$), during steady-state imbi-
 122 bition (brine fractional flow increasing with each step). The fluids in the system were
 123 brine (3.5 wt% KI) and decalin. The initial oil saturation after drainage was 86%. For
 124 further information see Lin et al. (2018a).

125 The second dataset - that we call Bentheimer Altered - used a sample that was very
 126 similar to the Bentheimer Unaltered, except that the wetting state was altered before
 127 the coreflood. Prior to the flow experiments, this sample was partially saturated with
 128 crude oil and heated at 80°C for 30 days in a wetting alteration process known as age-
 129 ing. The fluids in this case were brine (3.5 wt% KI, 1.09 wt% NaCl, 0.02 wt% $\text{MgCl}_2 \cdot 6\text{H}_2\text{O}$,
 130 0.11 wt% $\text{CaCl}_2 \cdot 2\text{H}_2\text{O}$) and decalin (Lin, Bijeljic, Berg, et al., 2019; Lin, Bijeljic, Krevor,
 131 et al., 2019). Five images at fractional flow steps $f_w = \{0.24, 0.50, 0.80, 0.90, 1\}$ were
 132 considered in this study. The initial oil saturation after drainage was 85%.

133 2.2 Multi-mineralogical system: experiments on Berea sandstone

134 2.2.1 Rock samples

135 Two Berea sandstone samples of 4 mm in diameter and 20 mm in length were drilled
 136 from the same core. This core has laminations of cemented calcite. The main mineral
 137 groups present were identified by scanning electron microscopy (SEM) operated in back
 138 scattered electron (BSE) mode and coupled with energy-dispersive X-ray spectroscopy
 139 (EDS) (Lai et al., 2015). Quartz grains constitute the majority of the rock matrix. The
 140 other mineral groups identified were clay group minerals (kaolinite, illite and smectite),
 141 sodium and potassium feldspars and small traces of minerals embedding metals. As with
 142 the Bentheimer, one of the samples was used unaltered by crude oil and is referred to
 143 as Berea Unaltered. The other sample underwent crude oil exposure after primary drainage
 144 and will be referred to as Berea Altered.

145 2.2.2 Fluids, fluid injection strategy, and wettability alteration

146 Two drainage-imbibition cycle experiments were performed. In the experiment in-
 147 volving Berea Unaltered, the fluids employed were brine (15 wt% KI in de-ionized wa-
 148 ter) and decane. The sample was firstly saturated with brine at atmospheric pressure
 149 and then pressurized at the injection pressure of 3.5 MPa. Decane was thus injected at
 150 a flow rate of $0.015 \frac{\text{ml}}{\text{min}}$, which corresponds to a capillary number $N_c \approx 10^{-7}$. The to-
 151 tal injected volume of decane was 2.5 ml. The initial oil saturation after drainage was
 152 larger than 95%. The injection was stopped for at least 4 hours in addition to the scan-
 153 ning time, before performing brine injection. 40 pore volumes were injected at a constant
 154 flow rate of $0.015 \frac{\text{ml}}{\text{min}}$.

155 In the experiment with the sample Berea Altered, the fluids employed were brine
 156 (15 wt% KI, 1.09 wt% NaCl, 0.02 wt% $\text{MgCl}_2 \cdot 6\text{H}_2\text{O}$, 0.11 wt% $\text{CaCl}_2 \cdot 2\text{H}_2\text{O}$) and an asian
 157 degassed crude oil with a density of 0.8592kg/m^3 and viscosity $9.4672 \text{mPa}\cdot\text{s}$. The crude
 158 has a total acid number (TAN) of 0.09mgKOH/g and a total basic nitrogen (TBN) of
 159 270.6mg/kg . The SARA (Saturates, Aromatics, Resing and Asphaltenes) analysis data
 160 is Sat = 44.00 wt%, Aro = 44.00 wt%, Res = 9.69 wt% and Asp = 2.31 wt%.

161 The sample was firstly saturated with brine. Crude oil drainage was then performed
 162 by setting a constant pressure gradient of 5 Mpa between the injection and the receiv-
 163 ing pumps, up to a total volume injection of 2.5 ml. The initial oil saturation was larger

164 than 95%. After drainage, the sample was then removed from the coreholder and stored
 165 immersed in crude oil in a sealed glass bottle. The glass bottle was put into an oven at
 166 a temperature of 80°C for 30 days. After the wettability alteration protocol, the sam-
 167 ple was mounted in the coreholder and waterflooding was performed, by injecting 40 pore
 168 volumes of brine at a constant flow rate of 0.015 $\frac{\text{ml}}{\text{min}}$.

169 In both the experiments, after waterflooding the injection was stopped and the sys-
 170 tem was allowed to equilibrate for 4 hours to a pressure of 3.5 MPa.

171 ***2.2.3 Imaging and Image processing of Berea sandstone: minerals and*** 172 ***fluids phase segmentation***

173 The samples were imaged with an FEI Heliscan microCT obtaining a voxel size of
 174 2.0 μm for a region of interest larger than the sample cross section and a vertical length
 175 of 8 mm. The projections were acquired while the sample was moving along a helical tra-
 176 jectory and a 1 mm thick aluminium filter was employed. The X-ray source voltage was
 177 set to 95 kV and the tube current to 70 mA. The raw images were reconstructed employ-
 178 ing an iterative back-projection algorithms provided by the scanner manufacturer. For
 179 both samples, images were acquired before the injection of any fluid (referred to as the
 180 dry scan) and after waterflooding.

181 The processing steps were the same for both samples. We filtered the dry scan and
 182 waterflooding image by non-local means filtering (Buades et al., 2005) and registered them.
 183 The greyscale dry scans were segmented using watershed segmentation (Beucher & Meyer,
 184 1993) into five phases: pore space, clay group minerals, quartz and feldspar group min-
 185 erals (that we refer to as quartz-feldspar), cemented calcite and others highly attenuat-
 186 ing minerals. The filtered waterflooding image was masked with the segmented pore space
 187 image, leading us to the segmentation of the two fluid phases (oil phase and brine phase)
 188 by simple thresholding. The region of interest of our analysis for each image was a cube
 189 of 1200 voxel side, i.e. 2.4 mm.

190 **2.3 Rock surface coverage as a measure of wetting: a model for water-** 191 **wet systems**

192 Consider a porous medium comprising two fluid phases, a wetting phase, w , and
 193 a non-wetting phase, o , e.g., oil, and a solid phase, s . Per unit volume of pore space, the
 194 reversible work required to increase the saturation of a non-wetting phase results in the
 195 creation of fluid-fluid interfaces, between wetting phase, non-wetting phase, and the solid
 196 (Morrow & Szabo, 1970; Bradford & Leij, 1997),

$$P_c dS_o = \sigma_{ow} dA_{ow} + \sigma_{os} dA_{os} + \sigma_{ws} dA_{ws} \quad (1)$$

197 P_c is the capillary pressure, S_i is the saturation with $S_o = 1 - S_w$, σ_{ij} is the interfa-
 198 cial tension between fluid or solid phase i and phase j , and A is the interfacial area per
 199 unit volume of pore space between phases.

200 The use of reversible work in the analysis is equivalent to limiting our considera-
 201 tion to equilibrium states of the system, i.e., $P_c(S_o)$ and $A_{ij}(S_o)$ at equilibrium. We ig-
 202 nore irreversible work that may be required in practice to move from one state to the
 203 next, e.g., due to transient processes (Berg et al., 2013; Morrow & Szabo, 1970). This
 204 is the assumption made when making use of capillary pressure characteristic curves as
 205 constitutive laws in the description of subsurface flow.

206 By integrating Eq.1, followed by algebraic operations and making use of the Laplace
 207 relationship, $P_c = 2\kappa\sigma_{ow}$, where κ is the mean interfacial curvature of the oil-brine in-
 208 terface, it is possible to derive the following (see the Supporting Information for a full

209 derivation):

$$A_{os}(S_o) = \frac{1}{\beta} \frac{\sigma_{ow}}{\sigma_{os} - \sigma_{ws}} \left(2 \int_{S'=0}^{S_o} \kappa dS' - \int_{S'=0}^{S_o} \frac{dA_{ow}}{dS'} dS' \right) \quad (2)$$

210 The terms inside the brackets represent the reversible work of desaturation and the cre-
 211 ation of oil-water interfacial area, respectively. The equation expresses the oil-solid in-
 212 terfacial area created from the excess energy available when subtracting the work required
 213 for the creation of fluid-fluid interfacial area from the work performed to increase the sat-
 214 uration of the non-wetting phase in the rock. The ratio of interfacial tensions, $\frac{\sigma_{ow}}{\sigma_{os} - \sigma_{ws}}$,
 215 is equivalent to $\frac{1}{\cos \theta}$ in a single capillary tube (θ is the contact angle). Without chang-
 216 ing sign entirely, the more wetting the solid is with respect to the non-wetting phase (the
 217 smaller the value of σ_{os}), the more interfacial area between the non-wetting phase and
 218 solid, A_{os} , will be created per unit of work. The parameter β represents a roughness fac-
 219 tor that accounts for the mismatch between the real surface area shared by each fluid
 220 and the solid surface and the one measurable by imaging, due to imaging resolution limit
 221 (Helgeson et al., 1984; White & Peterson, 1990).

222 2.4 Rock surface coverage characterisation by micro-CT imaging

223 In order to characterise rock surface coverage, the interfaces between mineral phases
 224 and fluid phases were identified. In the case of the Bentheimer datasets two groups of
 225 interfaces were identified, between oil and rock, and between brine and rock phases. In
 226 the case of the multi-mineral Berea sandstone, having produced segmented images with
 227 four mineral phases and two fluids, we identified a total of eight interface groups, i.e.,
 228 for each mineral and both fluid phases. Once an interface of interest was identified, a smooth
 229 surface was constructed through that interface by means of a generalized marching cubes
 230 algorithm.

231 We compare fluid surface coverage of different minerals by defining the fraction of
 232 the total area of that mineral in contact with a fluid:

$$a_{ij} = \frac{A_{ij}}{\sum_i A_{ij}} \quad (3)$$

233 where A_{ij} is the measured surface area per unit of pore volume shared by fluid i with
 234 solid j , respectively. The fractional definition of this property serves two purposes: to
 235 allow for the comparison of the specific wetting preference of different mineral groups
 236 with different total mineral-to-pore surface areas; to make the measurement more robust
 237 to the surface smoothing and to the image processing pipeline chosen.

238 3 Results and Discussion

239 3.1 Bentheimer sandstone: fluid coverage of chemically homogeneous 240 rock surfaces

241 The region of interest for the ten images considered (five for Bentheimer Unaltered
 242 and five for Bentheimer Altered) was divided into 90 cubic subvolumes of 300 voxels per
 243 side (voxel size $3.58 \mu m$). This allowed us to obtain a topological description of the wet-
 244 ting state of the system investigated. In each of the subvolumes, for each of the images
 245 and each of the datasets, fluid saturations, rock volume and fluid-coated interfacial ar-
 246 eas were computed.

247 The results obtained from the employment of our approach to wettability charac-
 248 terisation reconciled well with the authors' assumptions that Bentheimer Unaltered was
 249 water-wet (Lin et al., 2018a) and Bentheimer Altered was intermediate or mixed wet-
 250 ting to oil (Lin, Bijeljic, Berg, et al., 2019). Specific oil-rock interfacial area measurements
 251 are reported as a function of saturation for each of the subvolumes and for each of the

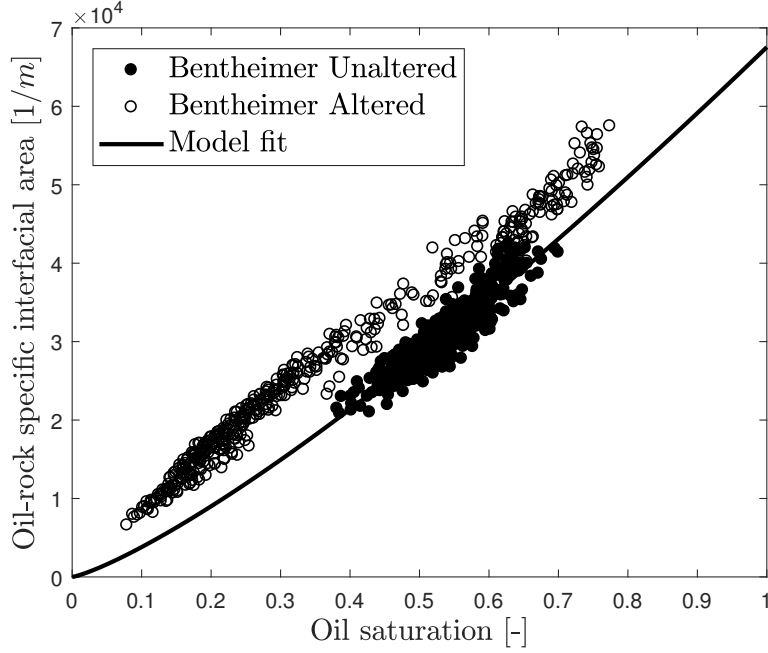


Figure 1. Oil-rock specific interfacial area measured in two Bentheimer sandstone datasets consisting of the X-ray micro-CT images of two steady-state imbibition experiments. For similar oil saturation values, the oil-coated specific interfacial areas are larger in the altered sample than in the unaltered one. The behaviour of the experimental data defined for Bentheimer Unaltered is reproduced by the model (Eq.2). For the details of the fitting process and the input parameters values, see the Supporting Information. The average oil-rock specific interfacial area and fluid saturation measured for each fractional flow considered are available in Table S1 (Supporting Information).

fractional flow considered in the two datasets Bentheimer Unaltered and Bentheimer Altered in Figure 1. For similar oil saturation values, in the intermediate-wet sample (Bentheimer Altered) rock surface coverage by oil is larger. As expected in a mixed or intermediate wet system, oil is more likely to coat the solid surface than in a water-wet system. Figure 1 also shows that the model we proposed for water-wet systems (Eq.2) well reproduces the behaviour of the measured specific oil-rock interfacial area datapoints in the Bentheimer Unaltered dataset. By fitting the model to the experimental data, we estimated $\frac{1}{\beta} \frac{\sigma_{ow}}{\sigma_{os} - \sigma_{ws}} = 0.07$. For a water-wet system $\frac{\sigma_{ow}}{\sigma_{os} - \sigma_{ws}} \geq 1$. This implies that the geometrical roughness factor $\beta \approx 10^0 - 10^3$, consistent with literature roughness factor values defined by comparing surface areas measured with BET to those estimated by X-ray micro-CT imaging for other sandstone rocks (Lai et al., 2015). For additional information on model fitting and the choice of input parameters, refer to the Supporting Information, where we also refer to Joekar-Niasar and Hassanizadeh (2012), Porter et al. (2009) and Raeesi et al. (2014).

3.2 Berea sandstone: the role of rock surface mineralogy in controlling the wetting state

In this case the region of interest was divided as the previous case in cubic subvolumes of 300 voxels side, for a total of 64 subvolumes. In each of the subvolumes fluid saturations, mineral volume fractions and specific mineral fluid coating were computed.

Table 1. Mineral volumetric composition and remaining fluid saturation (oil remaining saturation S_{or} , brine remaining saturation S_{wr}) after waterflooding from X-ray micro-CT images of the two Berea samples used in this study: Berea Unaltered (not aged by crude oil exposure) and Berea Altered (aged by crude oil exposure). The images were segmented into six phases: clay group minerals, quartz and feldspar (named quartz-feldspar phase), calcite cementation, other highly X-ray attenuating minerals, oil phase and brine phases.

	Berea Unaltered		Berea Altered	
	Mean [-]	St.Dev [-]	Mean [-]	St.Dev [-]
Clay	0.040	0.009	0.045	0.010
Quartz-Feldspar	0.840	0.046	0.813	0.043
Calcite	0.115	0.050	0.135	0.048
Others	0.006	0.004	0.006	0.004
S_{or}	0.572	0.050	0.239	0.071
S_{wr}	0.428	0.050	0.761	0.071

3.2.1 Mineral composition and fluid saturation

The segmentation of the images of the two Berea sandstone samples led to similar mineral compositions (Table 1). This confirmed that the mineral segmentation workflow employed is reproducible. The largest component of the rock matrix is the quartz-feldspar group minerals. Cemented calcite constitutes the second most abundant mineral by volume fraction in the samples. Due to the process through which this cementation likely formed, it is pore filling, exposing mineral surfaces only to poorly accessible regions of the pore space. Segmented clay group minerals are broadly distributed, either as patches on quartz and feldspar grains or as clay aggregates.

The injection of 40 pore volumes of brine led to distinct values of remaining fluid saturation between the unaltered and the altered samples. Berea Unaltered shows an average remaining oil saturation of 57%, while in Berea Altered oil displacement was more effective, leading to an average oil saturation of only 24%. Mixed-wet conditions are more favourable to the recovery of the oil phase as it has been observed extensively on larger coreflood tests (Salathiel, 1973). As observed for the Bentheimer datasets, the variability in saturation is larger for the sample that underwent the wettability alteration procedure.

3.2.2 Fluid arrangement in the pore space

A visual inspection of the greyscale images acquired after waterflooding for the two samples shows that the fluid arrangement differs. While in the unaltered sample, clay minerals are mainly filled with brine after the waterflooding, in the altered sample, brine is prevented from invading the small pores of the clay (Figure 2). Since clay aggregates mainly expose their surfaces to small pores, if clay minerals were still preferentially water-wetting we would expect brine to imbibe easily within these pores. On the contrary, the qualitative observation that these clay aggregates are mainly filled with oil suggests they have altered to an oil-wet state.

As shown for Bentheimer sandstone, we expect oil-coated surface area fraction to be positively correlated with oil saturation, i.e. the more oil in the pore space, the larger the fraction of mineral surface area contacted by oil. However, for both Berea Unaltered and Berea Altered this correlation is weak, as a consequence of the narrow range of fluid saturation in the experiment.

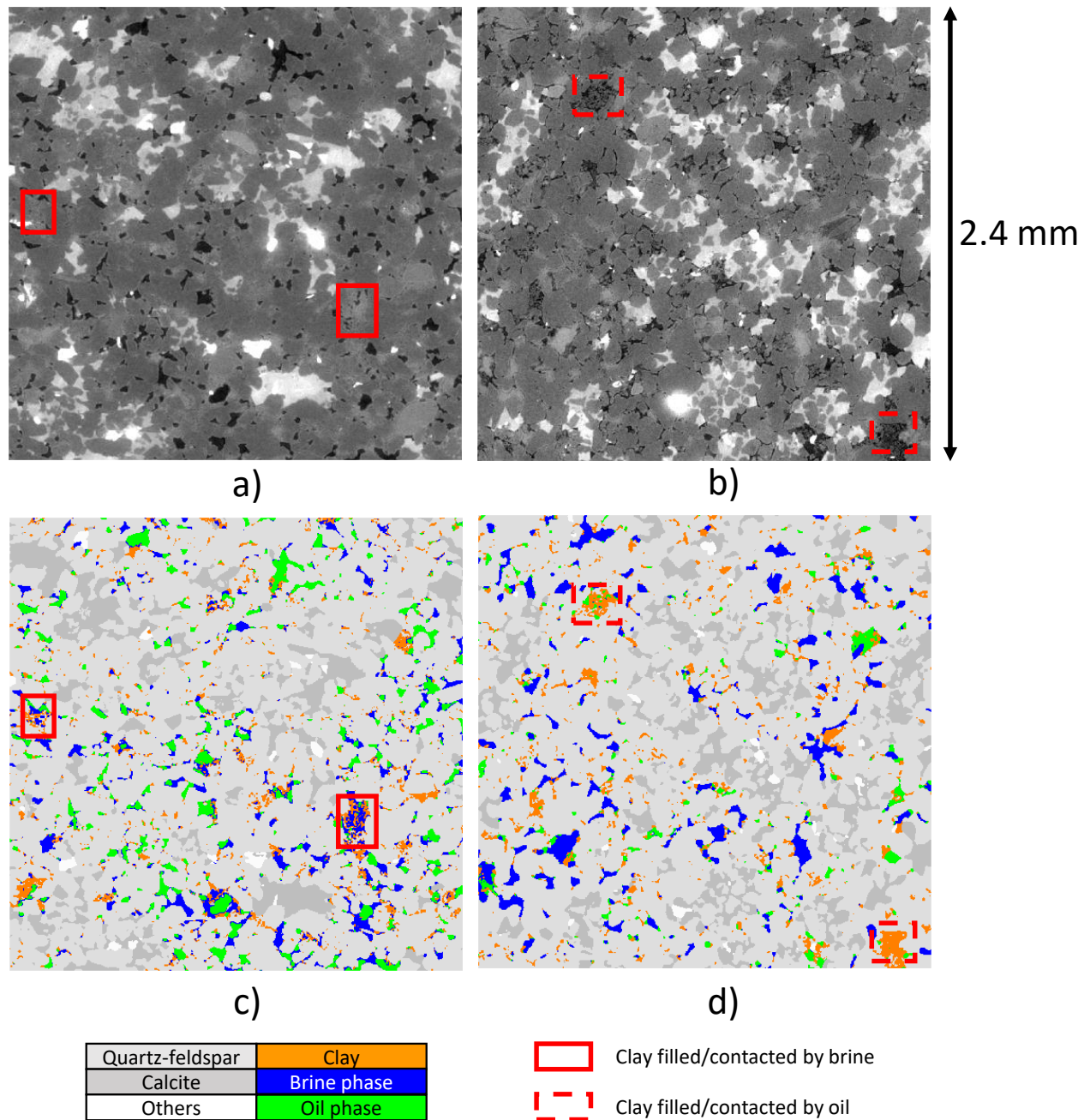


Figure 2. a) and b) show the greyscale images acquired after waterflooding of Berea Unaltered and Berea Altered, respectively (in the Supporting Information the respective dry scans can be found, Figure S1). c) and d) show the segmented respective of a) and b). a) and b) show the change in clay wetting preference due to the effectiveness of the ageing protocol in Berea Unaltered and Berea Altered, respectively. In the sample Berea Unaltered clay aggregates are readily invaded by brine during waterflooding. In contrast, in the aged sample Berea Altered, brine invasion is largely prevented by the oil-wetting behaviour of clay surfaces.

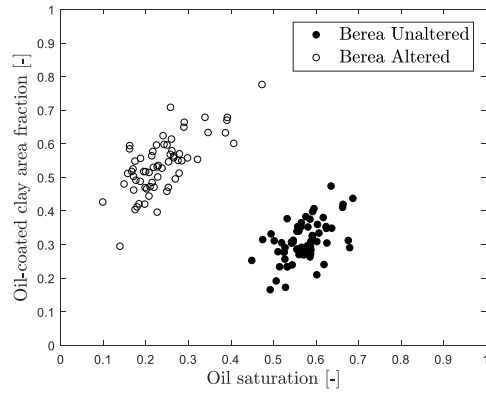
302 The oil-coated surface area fractions computed for Berea Unaltered suggest that
303 all mineral groups considered are preferentially wetting to brine (Figure 3). Average oil-
304 coated surfaces are always less than water coated surfaces even at high oil saturation.
305 The average oil-coated clay surface area fraction is smaller than the quartz-feldspar frac-
306 tion and this may be due to pore morphology and/or sub-resolution roughness. The small
307 pores found in these clays are preferentially imbibed by brine, due to the high capillary
308 pressure required for the non-wetting phase to occupy them. Similarly, calcite cement
309 mainly exposes its surface area to brine. This is a consequence of the capillary pressures
310 associated with the narrow pore regions that the cementation did not fill when it formed
311 (Figure 2). These findings are consistent with previous studies identifying these miner-
312 als as water-wet under experimental conditions similar to what we used (Blunt et al.,
313 2019; Khishvand et al., 2016; Singh et al., 2016). In the unaltered sample pore geom-
314 etry and rock texture are likely to be responsible for the differences in the oil-coated min-
315 eral surface area fractions encountered. The system is uniformly water-wet.

316 In contrast, rock mineral heterogeneities do control wettability alteration during
317 the ageing procedure. In Berea Altered, with a remaining oil saturation of 24%, 54% of
318 the clay surface area is coated by oil. This shows a strong change in the wetting pref-
319 erence of clay minerals, from water-wet to oil-wet. Even at lower oil saturation, there
320 is much higher surface area coverage of clay minerals by oil in the altered sample rela-
321 tive to the unaltered sample. Similarly, a large increase is observed for cemented calcite,
322 when results for Berea Unaltered are compared to those obtained for Berea Altered. On
323 the other hand, quartz and feldspar do not show as strong of a wettability change. The
324 reduced activity of quartz and feldspar surfaces during ageing compared to those of clay
325 and calcite is consistent with what has been observed in Alipour Tabrizy et al. (2011),
326 where pure powdered kaolinite and calcite were found more prone to wettability alter-
327 ation.

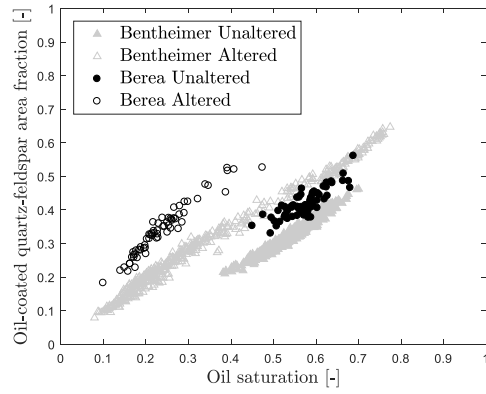
328 4 Conclusions

329 The analysis of rock mineral surface coverage by fluids can depict differences in the
330 wetting state of two fluid-phase systems. The solid surface covered by a fluid is positively
331 correlated with the saturation of that fluid. The particular relationship between fluid
332 saturation and fluid-mineral interfacial area depends on the wetting state of the system.
333 Considering the case of a uniformly water-wet system, we proposed a model that relates
334 rock coverage to fluid saturation, fluid-fluid interfacial curvature and fluid-fluid inter-
335 face extent, measurements more easily acquired with X-ray micro-CT imagery than al-
336 ternative approaches to *in situ* wetting characterization, e.g., contact angle. This model
337 was validated by observations made before and after wetting alteration on a mineralog-
338 ically homogeneous Bentheimer sandstone.

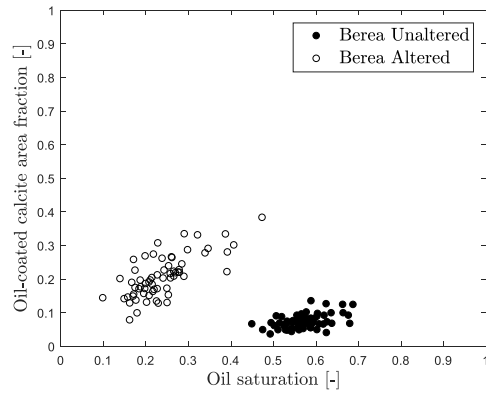
339 The measure of rock surface coverage allowed us to investigate the role that min-
340 eralogy plays in defining the wetting state of two sandstone rocks. In an untreated rock
341 sample with significant fractions of quartz, calcite, kaolinite and feldspar, fluid arrange-
342 ment and surface coverage after a drainage and imbibition displacement sequence were
343 consistent with a uniformly water-wet rock, regardless of local mineralogy. However, in
344 a sample previously exposed to crude oil at a temperature of 80°C for 30 days, miner-
345 alogical heterogeneity has been found responsible for heterogeneous wettability alteration
346 processes. Clay and calcite minerals were found more readily altered to an oil-wet state
347 than quartz and feldspar minerals. As a consequence, the sample wetting state was het-
348 erogeneous, mixed-wet, with the distribution of the wetting state controlled by the lo-
349 cal mineralogy.



a)



b)



c)

Figure 3. Oil-coated area fractions (a_{ij}) computed in the two Berea sandstone samples imaged after waterflooding. The average remaining oil saturation in Berea Unaltered is 57%. The average remaining oil saturation in Berea Altered is 24%. Quartz and feldspar minerals show a modest shift towards oil wetting. By comparison, clay and calcite minerals preferentially altered to an oil-wet state, with an average increase in the oil-coated area fraction of 74% and 184%, respectively. For the average and standard deviation values of the oil-coated area fractions (a_{ij}) see Table S2 in the Supporting Information. For reference, b) also reports the oil-coated area fractions (a_{ij}) computed for the two Bentheimer samples in b), being Bentheimer mainly constituted by quartz.

Acknowledgments

We gratefully acknowledge Shell Global Solutions International B.V. for permission to publish this work. The Unaltered Bentheimer sandstone data are available from Lin et al. (2018b). The Altered Bentheimer sandstone dataset are available from Lin et al. (2020). The Berea sandstone datasets are available from Garfi et al. (2020).

References

- Alhammadi, A. M., AlRatrou, A., Singh, K., Bijeljic, B., & Blunt, M. J. (2017). In situ characterization of mixed-wettability in areservoir rock at sub-surface conditions. *Scientific Reports*, *7*(1), 10753. Retrieved from <http://www.nature.com/articles/s41598-017-10992-w> doi: 10.1038/s41598-017-10992-w
- Alipour Tabrizy, V., Denoyel, R., & Hamouda, A. A. (2011). Characterization of wettability alteration of calcite, quartz and kaolinite: Surface energy analysis. *Colloids and Surfaces A: Physicochemical and Engineering Aspects*, *384*(1-3), 98–108. Retrieved from <http://dx.doi.org/10.1016/j.colsurfa.2011.03.021> doi: 10.1016/j.colsurfa.2011.03.021
- AlRatrou, A., Raeni, A. Q., Bijeljic, B., & Blunt, M. J. (2017). Automatic measurement of contact angle in pore-space images. *Advances in Water Resources*, *109*, 158–169. doi: 10.1016/j.advwatres.2017.07.018
- Anderson, W. (1987a). Wettability Literature Survey- Part 4: Effects of Wettability on Capillary Pressure. *Journal of Petroleum Technology*, *39*(10), 1605–1622. doi: 10.2118/16471-PA
- Anderson, W. (1987b). Wettability Literature Survey-Part 5: The Effects of Wettability on Relative Permeability. *Journal of Petroleum Technology*, *39*(12), 1605–1622. doi: 10.2118/16471-PA
- Andrew, M., Bijeljic, B., & Blunt, M. J. (2014). Pore-scale contact angle measurements at reservoir conditions using X-ray microtomography. *Advances in Water Resources*, *68*, 24–31. Retrieved from <http://dx.doi.org/10.1016/j.advwatres.2014.02.014> doi: 10.1016/j.advwatres.2014.02.014
- Berg, S., Ott, H., Klapp, S. A., Schwing, A., Neiteler, R., Brussee, N., . . . Others (2013). Real-time 3D imaging of Haines jumps in porous media flow. *Proceedings of the National Academy of Sciences*, *110*(10), 3755–3759. doi: 10.1073/pnas.1221373110
- Beucher, S., & Meyer, F. (1993). The morphological approach to segmentation: the watershed transformation. *Mathematical Morphology in Image Processing*, 433–481. Retrieved from <https://www.crcpress.com/Mathematical-Morphology-in-Image-Processing/Dougherty/p/book/9780824787240> doi: ExportDate6May2013
- Blunt, M. J., Jackson, M. D., Piri, M., & Valvatne, P. H. (2002). Detailed physics, predictive capabilities and macroscopic consequences for pore-network models of multiphase flow. *Advances in Water Resources*, *25*(8), 1069–1089.
- Blunt, M. J., Lin, Q., Akai, T., & Bijeljic, B. (2019). A thermodynamically consistent characterization of wettability in porous media using high-resolution imaging. *Journal of Colloid and Interface Science*, *552*, 59–65. Retrieved from <http://www.sciencedirect.com/science/article/pii/S0021979719305648> doi: <https://doi.org/10.1016/j.jcis.2019.05.026>
- Bradford, S. A., & Leij, F. J. (1997). Estimating interfacial areas for multi-fluid soil systems. *Journal of Contaminant Hydrology*, *27*(1), 83–105. Retrieved from <http://www.sciencedirect.com/science/article/pii/S0169772296000484> doi: [https://doi.org/10.1016/S0169-7722\(96\)00048-4](https://doi.org/10.1016/S0169-7722(96)00048-4)
- Buades, A., Coll, B., Matem, D., Km, C. V., Mallorca, P. D., Morel, J.-m., & Cachan, E. N. S. (2005). A non-local algorithm for image denoising. (0), 0–5.

- 403 Buckley, J. S. (1998). Wetting Alteration of Solid Surfaces by Crude Oils and Their
 404 Asphaltenes. *Revue de l'Institut Français du Pétrole*, 53(3), 303–312. doi: 10
 405 .2516/ogst:1998026
- 406 Buckley, J. S., & Liu, Y. (1998). Some mechanisms of crude oil/brine/solid interac-
 407 tions. *Petroleum Science and Engineering*, 155–160.
- 408 Buckley, S., & Leverett, M. (1942). Mechanism of fluid displacements in sands.
 409 *Transactions of the AIME*, 146, 107–116.
- 410 Bultreys, T., Boone, M. A., Boone, M. N., De Schryver, T., Masschaele, B., Van
 411 Hoorebeke, L., & Cnudde, V. (2016). Fast laboratory-based micro-computed
 412 tomography for pore-scale research: Illustrative experiments and perspec-
 413 tives on the future. *Advances in Water Resources*, 95, 341–351. Retrieved
 414 from <http://dx.doi.org/10.1016/j.advwatres.2015.05.012> doi:
 415 10.1016/j.advwatres.2015.05.012
- 416 Bultreys, T., De Boever, W., & Cnudde, V. (2016). Imaging and image-based fluid
 417 transport modeling at the pore scale in geological materials: A practical intro-
 418 duction to the current state-of-the-art. *Earth-Science Reviews*, 155, 93–128.
 419 Retrieved from <http://dx.doi.org/10.1016/j.earscirev.2016.02.001>
 420 doi: 10.1016/j.earscirev.2016.02.001
- 421 Coles, M. E., Hazlett, R., Muegge, E., Jones, K., Andrews, B., Dowd, B., ... W.E.,
 422 S. (1996). Developments in synchrotron x-ray microtomography with applica-
 423 tions to flow in porous media. *Society of Petroleum Engineers*, 1(4), 288–296.
 424 doi: 10.2118/36531-MS
- 425 Donaldson, E. C., Thomas, R. D., & Lorenz, P. B. (1969). Wettability Determina-
 426 tion and Its Effect on Recovery Efficiency. *SPE Journal*, 13–20. doi: 10.2118/
 427 2338-PA
- 428 Garfi, G., John, C. M., Berg, S., & Krevor, S. (2019, dec). The Sensitivity of Es-
 429 timates of Multiphase Fluid and Solid Properties of Porous Rocks to Image
 430 Processing. *Transport in Porous Media*. Retrieved from [https://doi.org/
 431 10.1007/s11242-019-01374-z](https://doi.org/10.1007/s11242-019-01374-z) doi: 10.1007/s11242-019-01374-z
- 432 Garfi, G., Lin, Q., Berg, S., & Krevor, S. (2020). *Berea sandstone: X-ray micro-*
 433 *ct imaging of waterflooding in a water-wet and a mixed-wet sample*. [http://
 434 www.digitalrockportal.org/projects/265](http://www.digitalrockportal.org/projects/265). Digital Rocks Portal. doi: 10
 435 .17612/Y7YD-H265
- 436 Garing, C., de Chalendar, J. A., Voltolini, M., Ajo-Franklin, J. B., & Benson, S. M.
 437 (2017). Pore-scale capillary pressure analysis using multi-scale X-ray micro-
 438 motography. *Advances in Water Resources*, 104, 223–241. Retrieved from
 439 <http://www.sciencedirect.com/science/article/pii/S0309170816305437>
 440 doi: <https://doi.org/10.1016/j.advwatres.2017.04.006>
- 441 Helgeson, H. C., Murphy, M., & Aagaard, P. E. R. (1984). Thermodynamic and
 442 kinetic constraints on reaction rates among minerals and aqueous solutions .
 443 II . Rate constants , effective surface area , and the hydrolysis of feldspar . ,
 444 48(c), 2405–2432.
- 445 Herring, A. L., Middleton, J., Walsh, R., Kingston, A., & Sheppard, A. (2017).
 446 Flow rate impacts on capillary pressure and interface curvature of con-
 447 nected and disconnected fluid phases during multiphase flow in sand-
 448 stone. *Advances in Water Resources*, 107, 460–469. Retrieved from
 449 <http://www.sciencedirect.com/science/article/pii/S0309170816307011>
 450 doi: <https://doi.org/10.1016/j.advwatres.2017.05.011>
- 451 Joekar-Niasar, V., & Hassanzadeh, S. M. (2012, sep). Uniqueness of Specific
 452 Interfacial Area–Capillary Pressure–Saturation Relationship Under Non-
 453 Equilibrium Conditions in Two-Phase Porous Media Flow. *Transport in
 454 Porous Media*, 94(2), 465–486. Retrieved from [https://doi.org/10.1007/
 455 s11242-012-9958-3](https://doi.org/10.1007/s11242-012-9958-3) doi: 10.1007/s11242-012-9958-3
- 456 Khishvand, M., Alizadeh, A. H., & Piri, M. (2016). In-situ characterization of
 457 wettability and pore-scale displacements during two- and three-phase flow

- 458 in natural porous media. *Advances in Water Resources*, *97*, 279–298. doi:
459 10.1016/j.advwatres.2016.10.009
- 460 Klise, K. A., Moriarty, D., Yoon, H., & Karpyn, Z. (2016). Automated contact an-
461 gle estimation for three-dimensional X-ray microtomography data. *Advances in*
462 *Water Resources*, *95*. doi: 10.1016/j.advwatres.2015.11.006
- 463 Lai, P., Moulton, K., & Krevor, S. (2015). Pore-scale heterogeneity in the min-
464 eral distribution and reactive surface area of porous rocks. *Chemical Geol-*
465 *ogy*, *411*(0), 260–273. Retrieved from [http://linkinghub.elsevier.com/](http://linkinghub.elsevier.com/retrieve/pii/S0009254115003290)
466 [retrieve/pii/S0009254115003290](http://linkinghub.elsevier.com/retrieve/pii/S0009254115003290) doi: 10.1016/j.chemgeo.2015.07.010
- 467 Lin, Q., Bijeljic, B., Berg, S., Pini, R., Blunt, M., & Krevor, S. (2020). *Pore-scale*
468 *imaging of multiphase flow at steady state for a mixed-wet bentheimer sand-*
469 *stone*. <http://www.digitalrockportal.org/projects/263>. Digital Rocks
470 Portal. doi: 10.17612/5WAP-ZM63
- 471 Lin, Q., Bijeljic, B., Berg, S., Pini, R., Blunt, M. J., & Krevor, S. (2019, Jun).
472 Minimal surfaces in porous media: Pore-scale imaging of multiphase flow in
473 an altered-wettability bentheimer sandstone. *Phys. Rev. E*, *99*, 063105. Re-
474 trieved from <https://link.aps.org/doi/10.1103/PhysRevE.99.063105> doi:
475 10.1103/PhysRevE.99.063105
- 476 Lin, Q., Bijeljic, B., Krevor, S. C., Blunt, M. J., Rücker, M., Berg, S., . . . Wilson,
477 O. B. (2019). A New Waterflood Initialization Protocol With Wettability
478 Alteration for Pore-Scale Multiphase Flow Experiments. *Petrophysics*, *60*(02),
479 264–272. Retrieved from <https://doi.org/> doi: 10.30632/PJV60N2-2019a4
- 480 Lin, Q., Bijeljic, B., Pini, R., Blunt, M., & Krevor, S. (2018b). *Pore-scale imag-*
481 *ing of multiphase flow at steady state for a bentheimer sandstone*. [http://www](http://www.digitalrockportal.org/projects/157)
482 [.digitalrockportal.org/projects/157](http://www.digitalrockportal.org/projects/157). Digital Rocks Portal. doi: 10
483 .17612/P7167R
- 484 Lin, Q., Bijeljic, B., Pini, R., Blunt, M. J., & Krevor, S. (2018a). Imaging and
485 Measurement of Pore-Scale Interfacial Curvature to Determine Capillary
486 Pressure Simultaneously With Relative Permeability. , 7046–7060. doi:
487 10.1029/2018WR023214
- 488 Morrow, N. R., & Szabo, J. O. (1970). Physics and Thermodynamics of
489 Capillary. *Industrial and Engineering Chemistry*, *62*(6), 32–56. doi:
490 10.1021/ie50726a006
- 491 Porter, M. L., Schaap, M. G., & Wildenschild, D. (2009). Lattice-Boltzmann simula-
492 tions of the capillary pressuresaturationinterfacial area relationship for porous
493 media. *Advances in Water Resources*, *32*(11), 1632–1640. Retrieved from
494 <http://www.sciencedirect.com/science/article/pii/S0309170809001328>
495 doi: 10.1016/j.advwatres.2009.08.009
- 496 Raeesi, B., Morrow, N., & Mason, G. (2014). Capillary pressure hysteresis behaviour
497 of three sandstones measured with a multistep outflow-inflow apparatus. *Va-*
498 *dose Zone Journal*, *13*(3). doi: 10.2136/vzj2013.06.0097
- 499 Rücker, M., Bartels, W. B., Singh, K., Brussee, N., Coorn, A., van der Linde, H. A.,
500 . . . Berg, S. (2019). The Effect of Mixed Wettability on Pore-Scale Flow
501 Regimes Based on a Flooding Experiment in Ketton Limestone. *Geophysical*
502 *Research Letters*, *46*(6), 3225–3234. doi: 10.1029/2018GL081784
- 503 Salathiel, R. (1973). Oil recovery by surface film drainage in mixed-wettability rocks.
504 *Petroleum Technology*, *25*, 1216–1224. doi: 10.2118/4104-PA
- 505 Scanziani, A., Singh, K., Blunt, M. J., & Guadagnini, A. (2017). Automatic method
506 for estimation of in situ effective contact angle from X-ray micro tomography
507 images of two-phase flow in porous media. *Journal of Colloid and Inter-*
508 *face Science*, *496*, 51–59. Retrieved from [http://dx.doi.org/10.1016/](http://dx.doi.org/10.1016/j.jcis.2017.02.005)
509 [j.jcis.2017.02.005](http://dx.doi.org/10.1016/j.jcis.2017.02.005) doi: 10.1016/j.jcis.2017.02.005
- 510 Singh, K., Bijeljic, B., & Blunt, M. (2016). Imaging of oil layers, curvature, and con-
511 tact angle in a mixed-wet and a water-wet carbonate rock. *Water Resource Re-*
512 *search*, *52*, 1716–1728. doi: 10.1002/2015WR018072

- 513 White, A. F., & Peterson, M. L. (1990). Role of Reactive-Surface-Area Characteriza-
514 tion in Geochemical Kinetic Models.
- 515 Zou, S., Armstrong, R. T., Arns, J.-Y., Arns, C., & Hussain, F. (2018). Exper-
516 imental and Theoretical Evidence for Increased Ganglion Dynamics During
517 Fractional Flow in Mixed-Wet Porous Media. *Water Resources Research*,
518 3277–3289. doi: 10.1029/2017WR022433